Effects of Pillar Depth and Shielding on the Interaction of Crossing Multitunnels

Charles W. W. Ng, F. ASCE[1]; Thayanan Boonyarak[2]* and David Mašín[3]

*Corresponding author

Type of paper: Technical paper

Information of the authors

[1] Chair Professor, Department of Civil and Environmental Engineering, The Hong Kong University of Science and Technology, Clear Water Bay, Kowloon, Hong Kong. E-mail: cecwwng@ust.hk

[2] PhD Candidate. Department of Civil and Environmental Engineering, The Hong Kong University of Science and Technology, Clear Water Bay, Kowloon, Hong Kong. E-mail: thayanan@connect.ust.hk

[3] Associate Professor, Faculty of Science, Charles University in Prague, Albertov 6, 128 43 Prague 2, Czech Republic. E-mail: masin@natur.cuni.cz

ABSTRACT:

Due to associated stress changes and induced ground movements, any new tunnel excavation may damage adjacent underground structures such as existing tunnels in congested cities. To evaluate the impact of new tunnel construction on nearby existing tunnels, a series of three-dimensional centrifuge model tests in dry sand were carried out together with numerical back-analyses using an advanced hypoplasticity constitutive model. The influences of the pillar depth-to-diameter ratio (P/D) on two-tunnel interaction and the effects of shielding on three-tunnel interaction were investigated. The maximum measured settlement of an existing tunnel caused by a new tunnel excavation at P/D of 0.5 underneath was about 50% larger than when P/D equals to 2.0. This is attributed to a smaller shear modulus, resulting from a larger reduction in confining stress of soil acting on the invert of the existing tunnel in the former than the latter. Different tunnel deformation mechanisms were observed with different P/D ratios. The existing tunnel was elongated horizontally when P/D equals to 0.5. This is because stress reduction in the horizontal direction was greater than that in the vertical direction. The stress relief caused by the new tunnel not only led to a reduction in the vertical stress at the invert but it also resulted in substantial stress reduction at the springline of the existing tunnel. On the contrary, the existing tunnel was elongated vertically as the new tunnel advanced at P/D of 2.0 since the reduction in stress in the vertical direction dominated. When the new tunnel was excavated underneath two perpendicularly crossing tunnels, the lower existing tunnel “shielded” the upper one from the influence of tunnel excavation. As a result, the settlement of the upper existing tunnel was 25% smaller than in the case without the shielding effects.

Author keywords: Multi-tunnel interaction; Three-dimensional centrifuge modeling; Three-dimensional numerical analysis; Pillar depth; Shielding effects.

INTRODUCTION

Existing tunnels in the ground may experience excessive deformation and their linings may show signs of cracking when new tunnels are excavated close to them. It is thus important to consider ground movements and stress changes when constructing new tunnels close to existing ones, especially in urban areas where more and more tunnels are being built with greater proximity to each other. Although the adverse effects of tunnel driving, such as excessive tunnel settlement, large angular distortion and cracking of tunnel linings, on an adjacent existing tunnel have been reported (Cooper et al., 2002; Mohamad et al., 2010), interpreting data from the field is particularly difficult due to variations in soil properties, in-situ stress conditions and tunneling workmanship.

Addenbrooke and Potts (2001) carried out a numerical parametric study of twin parallel tunnel interaction in plane strain conditions. The twin tunnels were excavated in both side-by-side and vertically stacked (piggyback) arrangements. In the case of the latter, the upper tunnel experienced increasing settlement and elongation in the vertical direction with decreasing pillar depth, which is defined as the clear vertical distance between two tunnels. However, their study did not simulate stress transfer in the longitudinal direction of the new tunnel. Thus the results may not carry over to the case of crossing tunnels.

Kim et al. (1998) investigated crossing-tunnel interaction under 1g conditions in clay. Two new tunnels were driven into a soil sample with a miniature shield machine and a hydraulic jack. Two different pillar depths between the existing and new tunnels were tested. They reported that the existing tunnel was compressed vertically because a jacking force was applied to install the liners of the new tunnels. Although different pillar depths were considered, the two new tunnels were driven above and below the existing tunnel one after the other. Thus, the effects of the second new tunnel excavation on the existing tunnel were likely affected by the presence of the first new tunnel.

Klar et al. (2005) investigated effects of tunneling on a pipeline using an elastic-continuum solution and a Winkler solution. A greenfield soil displacement that followed a Gaussian curve was imposed on the pipeline. Marshall et al. (2010) carried out centrifuge tests to investigate tunnel excavation perpendicularly underneath a pipeline in sand. Effects of volume loss caused by tunneling were simulated in plane strain conditions. They reported that soil-pipe stiffness was a major factor influencing the longitudinal bending moment of the pipeline. In addition, the presence of the pipeline significantly reduced the amount of shear strain induced above the pipeline. Addenbrooke and Potts (2001) also reported that the size and shape of the ground surface settlement trough in the case of piggyback tunnels differed from that in the greenfield case. Despite all these studies, the effects of shielding provided by an existing tunnel on the other adjacent existing tunnel are still not fully understood. The term "shielding effects" is used to describe the presence of an existing tunnel that reduces the influence of a new tunnel excavation on another adjacent existing tunnel.

Ng et al. (2013) investigated the three-dimensional interaction of perpendicularly crossing tunnels using centrifuge tests and numerical back-analysis. Their major objective was to study the individual effects of volume loss and weight loss on tunnel-tunnel interaction. A novel device called a "donut" was developed to simulate the effects of volume loss and mimic the removal of soil inside the tunnel in-flight. The settlements of the existing tunnel were observed to be larger when the effects of volume loss alone were simulated than when the effects of both volume loss and weight loss were modeled simultaneously. This is because weight loss caused stress relief, which resulted in a reduction in the amount of tunnel settlement induced by volume loss. However, only two-tunnel interaction and a single pillar depth were investigated in their study.

The major objectives of the present study are to investigate the influences of pillar depth on two-tunnel interaction and the effects of shielding on three-tunnel interaction. Three centrifuge tests are described and reported. A three-dimensional tunnel advancement technique considering the effects of both volume loss and weight loss was adopted (Ng et al., 2013). Three-dimensional numerical back-analyses of the centrifuge tests using a hypoplasticity constitutive model with small strain stiffness are also discussed.

THREE-DIMENSIONAL CENTRIFUGE MODELING

Test program

Figure 1a shows a typical plan view of a centrifuge model package used to investigate the interaction among multiple crossing tunnels in this study. The centrifuge tests were carried out in a geotechnical centrifuge located at the Hong Kong University of Science and Technology (Ng et al., 2001, 2002). By applying a centrifugal acceleration of 60 times that of the earth's gravity, a prototype stress condition can be recreated in the model. Each model tunnel was made from an aluminum alloy tube. The outer diameter (D) and the lining thickness were 100 mm and 3 mm, respectively, equivalent to 6 m and 180 mm in prototype scale. The scaling laws for the flexural stiffness of the lining per unit width and the flexural stiffness of the whole model tunnel are $1/N^3$ and $1/N^4$, respectively (Taylor, 1995). By assuming that the compressive strength of concrete (f'_c) is 50 MPa, Young's modulus (E_c) is estimated to be 33 GPa (ACI, 2011). Thus, the tunnel lining thicknesses are equivalent to 230 mm and 420 mm in prototype scale in the transverse and longitudinal directions of the existing tunnel, respectively. The existing tunnel was modeled as "wished-in-place" and each end was closed to keep soil out. The two ends of the existing tunnels were not connected to the model box and no additional fixity was imposed. Thus, the existing tunnel was not modeled as a continuous tunnel.

Figure 1b shows an elevation view of Test E2N3, whose objective was to investigate the effects of a new tunnel excavated perpendicularly beneath an existing tunnel. In this test, the C/D ratios of the existing tunnel and the new tunnel were 2.0 and 3.5 respectively, whereas the pillar depth-to-diameter ratio (P/D) was 0.5. These correspond respectively to the cover depths of the existing tunnel and the new tunnel of 12 m and 21 m in prototype, and the pillar distance of 3 m. Note that some of the measured results of this test have been reported by Ng et al. (2013).

In Test E2N5 (see Fig. 1c) which was designed to investigate the influence of P/D on how the existing tunnel might respond to the new tunnel excavation, a P/D of 2 instead of 0.5 was used. In Test E2,3N5 (refer to Fig. 1d) which featured two existing tunnels above the new one, the shielding effects of the lower existing tunnel were studied by comparing the results with those from Test E2N5.

According to Jacobsz et al. (2004), the influence zone of tunneling in sand was found to be in parabolic shape projecting 45° from the invert of the tunnel to the ground surface. By adopting this finding, the influence zone of the new tunnel excavation was estimated to be located within the boundary of the existing tunnel.

In-flight tunneling simulation technique

Figure 2a shows the new model tunnel used in each centrifuge test. Six “donuts” (Ng et al., 2013) with each representing an excavation length of 0.6D were adopted to simulate the effects of three-dimensional tunnel advancement in-flight. Both ends of the new tunnel were closed to keep soil out.

Figure 2b shows a cross sectional view of a “donut” which consisted of an aluminum alloy tube serving as the tunnel lining, an outer rubber membrane and an inner rubber membrane. During model preparation, each rubber membrane was filled with a heavy fluid ($ZnCl_2$) having the same density as the soil in each test. Volume loss equivalent to 2% was simulated by controlling the outflow of the heavy fluid from the outer membrane. Likewise, weight loss was simulated by draining an amount of heavy fluid equivalent to the weight of soil used in each test from the inner membrane. Each “donut” was connected with drainage tubes to a corresponding drainage valve. Each valve was regulated in-flight one after another allowing outflow of the heavy fluid to simulate the effects of tunnel advancement. The heavy fluid that was drained away was collected in a reservoir (refer to Fig. 1a).

Model preparation

Dry silica Toyoura sand was used in each centrifuge test. In previous studies, grain size effects on soil-tunnel interaction were considered insignificant when the ratio of tunnel diameter to average particle size was larger than 175 (Garnier et al., 2007). In this study, the ratio of model tunnel diameter (100 mm) to average particle size (0.17 mm, Ishihara, 1993) was 588.

A dry pluviation technique was adopted to prepare the soil sample in each test. A drop height of 500 mm and a pluviation rate of about 100 kg/hour were used to control the density of the soil sample. The density achieved in Tests E2N3, E2N5 and E2,3N5 were 1529 kg/m^3 (relative density, D_r = 64%), 1532 kg/m^3 (D_r = 65%) and 1535 kg/m^3 (D_r = 66%), respectively. According to a study on the homogeneity of pluviated sand samples in centrifuge tests, variations in dry density within ± 0.5% or ± 8 kg/m^3 are acceptable (Garnier, 2001).

Each existing tunnel was placed after the level of pluviated sand reached the designed height. By using some thin wires and a temporary structural beam above, the new tunnel was “wished-in-place” in position. These wires and the beam were removed after the pluvial deposition reached the bottom of the new tunnel to support it (refer to Fig. 2a).

Instrumentation

Figure 3a shows the types and locations of instruments installed in the existing tunnel. To measure tunnel settlement, linear variable differential transformers (LVDTs) were connected to the crown of the existing tunnel at various points via extension rods. Each extension rod was made of an aluminum alloy housed in a hollow aluminum alloy tube in order to reduce friction with the surrounding soil. In Test E2N3, the LVDTs measuring settlement of the existing tunnel were all installed along one half of that tunnel and the maximum distance of the extension rods from the centerline of the new tunnel was 4D (see the schematic diagram in Fig. 3). In Tests E2N5 and E2,3N5, the extension rods were placed along the length of the existing tunnel and were within a distance of 3D from the centerline of the new tunnel. The LVDTs were arranged differently in Tests E2N5 and E2,3N5 to observe the response of the existing tunnel near the centerline of the new tunnel, where maximum tunnel settlement was expected to occur.

Figure 3b shows potentiometers installed inside the existing tunnel at the location directly above the new tunnel. Four potentiometers were placed at the crown, at each springline and at the invert to measure tunnel deformation. A potentiometer is a three-terminal resistor that measures a change in resistance with a change in the travel distance of a slider (Todd, 1975). The accuracy of the potentiometers used in this study was estimated to be within ±0.017 mm in model scale (equivalent to ±1 mm in prototype scale) by considering the standard deviation of the data once the centrifugal acceleration had reached 60g prior to tunnel excavation.

Eight sets of foil strain gages were attached to both inner and outer surfaces of the lining of the existing tunnel at a spacing of about 45° around of the circumference. The strain gages having a gage factor of 2 were connected into a full Wheatstone bridge to compensate for temperature effects. In Test E2,3N5, potentiometers and strain gages in the transverse direction were also installed in the lower existing tunnel at the location directly below the upper existing tunnel.

Figure 3c shows a typical longitudinal section view of the existing tunnel. Four potentiometers were mounted on a plate, which was connected to a frame that was fixed to the lining of the existing tunnel. A total of 19 sets of semiconductor strain gages were attached along the length of the existing tunnel at the crown and invert at a typical spacing of 50 mm. The strain gages in the longitudinal direction of the existing tunnel were connected into a full Wheatstone bridge, having a gage factor of 140. Different types of strain gages were used in the longitudinal and transverse directions of the existing tunnel because the semiconductor ones are easily damaged during installation and so cannot be attached to the inner surface of the tunnel lining.

Test procedure

The model package was transferred to the centrifuge platform after model preparation and transducer calibration. An initial reading was taken from each transducer once the centrifuge had spun up to an acceleration of 60g and the transducers had stabilized, prior to the advancement of the new tunnel. Subsequently, the six stages of tunnel excavation proceeded in-flight (see Fig. 2a) one after another. In each stage of tunnel advancement, the transducers were allowed to stabilize before proceeding to the next stage. Once the tunnel was excavated, the centrifuge was gradually spun down.

THREE-DIMENSIONAL NUMERICAL BACK-ANALYSIS

The objective of numerical back-analysis is to understand the stress transfer mechanism and strain induced in the soil during the crossing multi-tunnel interaction. The numerical analysis is necessary because stress changes and strain induced in the soil around the tunnel could not be measured easily and accurately in the three-dimensional centrifuge model tests.

A commercial finite element program PLAXIS 3D 2012 (Brinkgreve et al., 2012) was adopted to back-analyze centrifuge test results. Soil was represented using an open-source hypoplastic model implementation (Gudehus et al., 2008).

Finite element mesh and boundary conditions

Figure 4a shows the three-dimensional finite element mesh for case E2N3. The dimensions of the mesh and tunnel configuration in each numerical run were identical to that in each centrifuge test. A plane of symmetry was defined at X/D of 0. The boundary conditions adopted in the finite element analysis were roller support on the four vertical sides and pin support at the base of the mesh. The soil was modeled using a 10-node tetrahedral element.

The closest distances from the side and the bottom boundaries to the tunnels were 3.5D and 1.5D, respectively. To justify any effect of mesh size on crossing-tunnel interaction, an additional sensitivity numerical analysis was carried out by doubling the width and the depth of the original mesh. The differences between computed results obtained from the original and the extended meshes are generally less than 6%.

Figure 4b shows some details of the two perpendicularly crossing tunnels in case E2N3. The existing tunnel and the lining of the new tunnel were modeled as “wished-in-place” by activating the tunnel lining and deactivating soil elements inside the tunnel in the initial stage. An additional constraint was adopted for the tunnel lining at the plane of symmetry. Each edge of the tunnel lining at the plane of symmetry was allowed neither translational movement in the “X” direction nor rotation around the “Y” and “Z” axes (i.e., u_x, ϕ_y and ϕ_z = 0). The tunnel lining was modeled using a 6-node elastic plate element.

Constitutive model and model parameters

Dry Toyoura sand was modeled using a hypoplasticity constitutive model with small strain stiffness. Hypoplasticity are non-linear constitutive models developed to predict the behaviour of soil (von Wolffersdorff, 1996; Gudehus and Mašín, 2009; Mašín, 2012). Small-strain stiffness or an intergranular strain concept was proposed by Niemunis and Herle (1997) to incorporate strain-dependent stiffness and the effects of recent stress history in a hypoplasticity model.

Hypoplasticity is a particular class of soil constitutive model characterized by the following rate formulation:

$$\overset{0}{T} = f_s(L : D + f_d N\|D\|)$$

where $\overset{0}{T}$ is a stress rate tensor, D is a strain rate tensor, L is a fourth order tensor, N is a second-order tensor, f_s is a barotropy factor including the influence of mean stress and f_d is a pyknotropy factor including the influence of relative density.

The basic hypoplastic model requires eight material parameters (ϕ_c, h_s, n, e_{d0}, e_{c0}, e_{i0}, α, β). ϕ_c is the critical state friction angle, which can be calibrated using the angle of repose test. The parameters h_s and n describe the slope and shape of limiting void ratio lines; that is, isotropic normal compression line, critical state line and minimum void ratio line. Parameters e_{d0}, e_{c0} and e_{i0} specify positions of these lines in the mean stress versus void ratio diagram. The parameters h_s, n and e_{c0} can be calibrated using oedometric test on loose sand sample. The parameters e_{d0} and e_{i0} can typically be estimated using empirical correlations. Finally, the model requires parameter α specifying peak friction angle and parameter β specifying shear stiffness. These parameters can be estimated using triaxial shear test.

The intergranular strain formulation or small strain stiffness requires five additional parameters, namely m_R, m_T, R, β_r and χ. Parameters m_R and m_T specify very small strain shear stiffness upon 180° and 90° change of strain path direction, respectively. Parameter R specifies the size of elastic range measured in the strain space; β_r and χ specify the rate of stiffness degradation with strain.

To determine model parameters, a critical state friction angle (ϕ_c) and parameters controlling void ratios (h_s, n, e_{d0}, e_{c0} and e_{i0}) were adopted based on calibration results reported by Herle and Gudehus (1999). Exponent α, exponent β and small strain stiffness parameters (m_R, m_T, R, β_r and χ) were calibrated by curve fitting the triaxial test results with local strain measurement and bender element reported by Yamashita et al. (2000, 2009). To initialize the stress conditions, the coefficient of at-rest earth pressure (K_0) was assumed to be 0.5. The model parameters are summarized in Table 1.

The tunnel lining was modeled as a linear elastic material. Its Young's modulus, density and Poisson's ratio were assumed to be 69 GPa, 2700 kg/m^3 and 0.33, respectively.

Mašín (2009) and Svoboda et al. (2010) adopted hypoplasticity constitutive model with small strain stiffness to predict greenfield settlement trough caused by a single tunnel excavation. It was found that the computed ground settlements were in a reasonable agreement with those from field observations.

Numerical modeling procedure

The procedure of numerical modeling basically followed that in the centrifuge tests. Drained effective stress analysis was adopted as every test was carried out in dry sand. The numerical simulation procedure is as follows:

1. Create the initial conditions as follows:
   1.1 Specify the void ratio in 1g conditions.
   1.2 Set the intergranular strain of soil elements to zero (i.e., no deformation at the initial stage).

1.3 Activate the lining of the existing and new tunnels to simulate "wished-in-place" tunnel lining.

1.4 Deactivate the soil elements inside the existing tunnel and some parts inside the new tunnel (see Fig. 4a).

1.5 Initialize stress under 1g conditions with K_0 equaling 0.5.

2. Increase the unit weight of soil and tunnel lining by 60 times that under 1g conditions to simulate rise in centrifugal acceleration.
3. Excavate new tunnel by simulating the effects of both volume loss and weight loss as follows:

3.1 To simulate the effects of 2% volume loss, the surface contraction technique (a utility available in the PLAXIS software) was used. This technique applies a uniform radial contraction on the tunnel lining. It should be noted that this numerical simulation technique does not represent a perfect match to that of centrifuge model tests. However, the discrepancy between the numerical and centrifuge simulation techniques should not affect any key conclusion obtained from this study significantly since the volume loss simulated in both numerical and physical modeling is identical.

3.2 Simulate the effects of weight loss by removing (i.e., deactivating) the soil elements (with the same unit weight as the heavy fluid used in the centrifuge test) inside the tunnel.

3.3 Restrain soil movement in the longitudinal direction of the new tunnel by applying a roller support to the tunnel face.

4. Advance the new tunnel by a distance of 0.6D in each excavation stage by repeating step 3 above for a total distance of 3.6D in six stages.

Numerical parametric study of tunneling in greenfield conditions

In addition to the numerical back-analysis of crossing-tunnel interaction, two additional numerical runs were carried out to investigate the effects of tunnel excavation on ground displacements in greenfield sites. In these two greenfield runs, all the geometries, boundary conditions and numerical procedures of tunneling are identical to those in the numerical back-analysis, except no existing tunnel is present in the two additional analyses.

INTERPRETATION OF RESULTS

Measured and computed results reported in this study are expressed in prototype scale unless stated otherwise.

Settlement of the existing tunnel

In order to compare results from this study with a case history, the tunnel settlement was normalized by the diameter of the new tunnel. Figure 5 compares the measured and computed normalized settlements of the existing tunnel at the end of tunnel advancement.

The maximum measured tunnel settlement in Test E2N3 was about 0.3%D (i.e., 18 mm), which exceeds the recommended serviceability limit of 15 mm (LTA, 2000). For the two-tunnel interaction, the maximum measured tunnel settlement in Test E2N3 (i.e., P/D of 0.5) was about 50% larger than that in Test E2N5 (i.e., P/D of 2). The larger tunnel settlement in Test E2N3 was mainly due to a larger reduction in vertical stress and lower normalized soil stiffness along the invert of the existing tunnel. Detailed explanations are given in the section incremental normal stress acting on the existing tunnel.

As for the three-tunnel interaction, the maximum measured settlement of the upper existing tunnel in Test E2,3N5 was about 25% smaller than that in Test E2N5 (provided that P/D of 2 for both tests) due to the presence of the lower existing tunnel (i.e., shielding effects). Further away from the centerline of the new tunnel, the difference in tunnel settlement between Tests E2N5 and E2,3N5 narrowed.

The induced tunnel gradient can be deduced from the slope of measured tunnel settlements. The largest induced tunnel gradient of 1:1600 was observed in Test E2N3, where the largest tunnel settlement occurred. The maximum induced tunnel gradients of the three tests all fell within the recommended limit of 1:1000 (LTA, 2000; BD, 2009).

In Test E2N3, the computed tunnel settlements were underestimated by 16 % at the location directly above the new tunnel. On the other hand, they were overestimated in Tests E2N5 and E2,3N5 by 8 % and 12 %, respectively, at the same location. This discrepancy may be due to the fact that some model parameters were obtained from the literature and empirical relationships. Although there were discrepancies between the measured and the computed results, both results show the same trend.

To assist in the interpretation of settlements of the existing tunnel, subsurface settlements caused by tunneling in the greenfield site are included and compared. As expected, the subsurface settlements due to the shallower tunnel excavation (N3) are larger than those caused by the deeper tunnel (N5). This is because N3 has a smaller C/D than that of N5 tunnel. It is well-understood that induced subsurface settlement is larger when tunneling at a shallower depth (i.e., reducing C/D), as reported by many researchers such as Mair and Taylor (1997) and Marshall et al. (2012). Similarly, it is expected that a larger tunnel settlement in Test E2N3 than that in Test E2N5. This is because the new tunnel excavation in the former test was shallower (i.e., smaller C/D) than that in the latter test.

Soil stiffness along the invert of the existing tunnel

To explain the difference in tunnel settlement among the three cases, the normalized soil stiffness along the invert of the existing tunnel was calculated as shown in Figure 6. The normalized soil stiffness was considered before tunnel excavation (once the centrifugal acceleration had reached 60g) and after tunnel completion. Secant shear moduli (G_{before} and G_{after}) were calculated from deviatoric stress and deviatoric strain ($G = q/3\varepsilon_s$) at the end of each stage. The normalized soil stiffness differed among the three cases because the hypoplasticity model can simulate the dependence of stiffness on the state, strain and recent stress history of the soil.

In terms of two-tunnel interaction, the normalized shear modulus was lower in case E2N3 than that in case E2N5 at the center of the existing tunnel (X/D of 0), resulting in a larger tunnel settlement (see Fig. 5). This is because the reduction in confining stress due to tunnel excavation was larger in the former than in the latter. Another reason for a larger reduction in mobilized shear modulus in E2N3 than that in E2N5 was due to higher shear strain mobilized in the former than the latter case. Similar results were also reported by Marshall et al. (2012) who found that shear strains in soil induced by tunnel excavation at a smaller C/D ratio was greater than that caused by a tunnel advanced at a larger C/D ratio. More explanations are given in the sections under incremental normal stress acting on the existing tunnel and induced deviatoric strain of soil.

An increase in shear modulus of soil was observed in cases E2N3 and E2N5 at an offset distances between 2D and 4D from the center of the existing tunnel. This is because the confining stress was increased due to stress redistribution, leading to the increase in soil stiffness. It is obvious that stress redistribution was necessary to maintain equilibrium.

As for three-tunnel interaction, there was almost no change in normalized stiffness at the centerline of the new tunnel in case E2,3N5 whereas the normalized stiffness was significantly reduced in case E2N5 (given that P/D of 2 in both tests). The minimum normalized stiffness in case E2,3N5 was found at an offset distance of 0.5D, which is the offset distance of the springline of the lower existing tunnel, due to the shielding effects of the lower existing tunnel.

Induced strain and shear stress in the longitudinal direction of the existing tunnel

Figure 7 compares the measured and computed strain induced along the invert of the existing tunnel at the end of tunnel advancement. The positive and negative signs denote induced tensile strain and induced compressive strain at the invert of the existing tunnel, respectively.

Due to differential settlement of the existing tunnel, sagging moment was induced directly above the new tunnel. As a result, tensile strain was induced at the invert of the existing tunnel. The measured maximum induced tensile strain of 152 με was found in Test E2N3, exceeding the cracking tensile strain of 150 με for unreinforced concrete (ACI, 2001). The measured maximum induced tensile strain in Test E2N5 (127 με) was 16% smaller than that in Test E2N3, where the former test had a larger P/D than the latter test. The measured maximum induced tensile strain in the upper existing tunnel in Test E2,3N5 (86 με) was 36% smaller than that in Test E2N5. This is due to shielding effects provided by the lower existing tunnel.

The induced strain in the longitudinal direction of the existing tunnel was consistent with the tunnel settlement in every test (refer to Fig. 5). The possible reason for discrepancies between the measured and computed results has been discussed previously under the section of settlement of the existing tunnel.

Shear stress acting on the tunnel lining was deduced by differentiating bending moment, which was converted from induced strain along the invert of the existing tunnel. At a given concrete compressive strength (f'_c) of 50 MPa and a reduction factor of 0.55, the allowable shear stress was estimated to be 660 kPa (ACI, 2011). The maximum deduced shear stress in Tests E2N3 (for both measured and computed results) exceeded the allowable limit, suggesting that the tunnel lining may crack.

There was a high possibility that cracking would occur when the tunnel was excavated at P/D of 0.5 (Test E2N3) as the induced tensile strain and shear stress exceeded the cracking tensile strain and the allowable shear stress, respectively.

Induced strain in the transverse direction of the existing tunnel

Figure 8 shows comparison between measured and computed strains induced at the outer surface of the existing tunnel in the transverse direction. As the strain induced in the first three excavation stages (i.e., from Y/D of -1.5 to -0.3) was smaller than that induced in the last three excavation stages (i.e., from Y/D of 0.3 to 1.5) and to simplify presentation, the results from the former are not shown.

In Test E2N3 (Fig. 8a), induced compressive strain was at shoulders, the right knee and the invert. Tensile strain was induced at both springlines. The induced strain in Test E2N3 indicates that the existing tunnel was elongated horizontally. To verify this horizontal elongation, tunnel deformation is shown and discussed in the next section. It can be seen that the computed strains induced in the transverse direction are consistent with the measured results.

Strain induced by tunneling caused tunnel deformations in different directions in Test E2N3 and Test E2N5 (Fig. 8b), where the former test had a smaller P/D than the latter test. In Test E2N5 tensile strain was induced at the crown and invert while compressive strain was induced at both springlines. Larger compressive strain and tensile strain were induced at both springlines and the invert, respectively, when Y/D was 0.9D than at the end of tunneling. The induced strain in Test E2N5 suggests that the existing tunnel was elongated vertically. The tunnels deformed in different directions in Tests E2N3 and E2N5 because of the varying incremental normal stresses acting on the existing tunnel with different P/Ds. More explanations are given later.

In Test E2,3N5 the P/D between the new tunnel and the upper existing tunnel was 2, identical to that in Test E2N5. Thus, the strain induced in the upper existing tunnel in Tests E2,3N5 (Figure 8c) and that induced in the existing tunnel in Test E2N5 (Figure 8b) were similar in terms of both magnitude and trend. As expected, the two tunnels were both elongated vertically.

Induced strain in the lower existing tunnel in Test E2,3N5 is shown in Figure 8d. Compressive strain was induced at the crown and both springlines while induced tensile strain was found at the shoulders, knees and invert. The induced strain suggests that the lower existing tunnel was elongated vertically.

Given that the induced compressive strain equaled the induced tensile strain on opposite surfaces of the tunnel lining, the tensile strain was at the maximum of 170 $\mu\varepsilon$ at the right springline on the inner surface of the existing tunnel in Test E2,3N5 (refer to Fig. 8d). This induced tensile strain exceeded the cracking tensile strain of 150 $\mu\varepsilon$ (ACI, 2001), suggesting that the inner surface of the tunnel lining may crack.

Deformation of the existing tunnel

Figure 9a shows the change in the normalized diameter of the existing tunnel ($\Delta D/D_0$), where D_0 is the initial diameter of the tunnel, in the vertical direction at the end of tunnel construction. According to the measured results, there was a reduction in the tunnel diameter in the vertical direction in Test E2N3 (P/D of 0.5), but the existing tunnel in Test E2N5 (P/D of 2) was vertically elongated. This is because stress reduction on the existing tunnel in the horizontal direction was larger than that in the vertical direction in the former test with a smaller P/D ratio. Details of stress changes at the existing tunnel are illustrated and discussed in the next section. It should be pointed out that stress relief caused by the new tunnel excavation not only led to a reduction in vertical stress but also it resulted in substantial stress reduction at each springline of the existing tunnel. On the other hand, when the new tunnel was located further away from the existing tunnel (i.e., P/D of 2), stress relief was dominated in the vertical direction and it mainly affected the invert of the existing tunnel, leading to the elongation of it.

Similar to that of Test E2N5, the upper existing tunnel was elongated in the vertical direction in Test E2,3N5, which has the same P/D ratio resulting in a larger reduction in the vertical than the horizontal stress. On the other hand, the lower existing tunnel in Test E2,3N5 was also elongated vertically even though the P/D was 0.5. This is because the invert of the lower existing tunnel was closest to the new tunnel, resulting in a sharp reduction in the vertical stress at the invert. The computed results are generally consistent with the measured tunnel deformations. Further explanations of stress acting on each existing tunnel are given in the next section.

By considering the computed subsurface settlements in greenfield conditions shown in Figure 5, it is evident that the subsurface settlement near the new tunnel (N3) was 33% larger than that caused by the deeper new tunnel (N5). This is consistent with results reported by Mair and Taylor (1997). Accordingly, the settlement induced at the invert of the existing tunnel was larger in Test E2N3 than that in Test E2N5.

Figure 9b shows the change in the normalized diameter of the existing tunnel in the horizontal direction. Both measured and computed results reveal that the existing tunnel was elongated horizontally in Test E2N3. This is because stress reduction on the existing tunnel in the horizontal direction was greater than that in the vertical direction. On the other hand, the diameter in each existing tunnel in Tests E2N5 and E2,3N5 was reduced horizontally as the decrease in the vertical stress was larger than the horizontal stress. The results of tunnel deformation in each case are consistent with the induced strains in the transverse direction of the existing tunnel (see Fig. 8).

BTS (2000) recommended that the difference between the maximum and minimum diameters of a tunnel should be within 2% [i.e., $(D_{max} - D_{min})/D_0 \leq 2\%$]. For the cases considered in this study, it can be seen in Figure 9 that the deformations of the existing tunnels due to tunnel excavation are still within the allowable limit.

Incremental normal stress acting on the existing tunnel

Figure 10 shows the computed incremental normal stress acting on the existing tunnel in the transverse direction at the location directly above the new tunnel (i.e., X/D of 0). The incremental stress in this study is defined as the difference between the stress at the end of tunnel excavation and that when centrifugal acceleration had reached 60g. Incremental normal stresses acting on the existing tunnel are obtained from the numerical back-analysis only.

In case E2N3 (see Fig. 10a), normal stress increased gradually at the crown as the new tunnel advanced. This is because stress was transferred in the longitudinal direction of the new tunnel to maintain stress equilibrium (Ng and Lee, 2005). At both springlines, there was a reduction in normal stress. At the invert, once the new tunnel approached the existing tunnel (i.e., Y/D of -0.3), a slight increase in normal stress was observed. As the new tunnel advanced further (i.e., from Y/D of 0.3 to 1.5), normal stress dropped sharply.

In case E2N5 (see Figure 10b), there was an increase in normal stress at the crown. At both springlines, the reduction in normal stress was smaller than that in case E2N3 as the P/D for the latter was smaller. At the invert, normal stress reduced substantially as the new tunnel advanced.

The fact that the existing tunnel deformed in different directions in cases E2N3 and E2N5 (refer to Fig. 9) can be explained by considering change in stress in the horizontal and vertical directions. In case E2N3, the decrease in stress in the horizontal direction was larger than that in the vertical direction at the end of tunneling, resulting in elongation of the existing tunnel in the horizontal direction. On the other hand, reduction in the vertical stress was larger than the horizontal stress in the case E2N5 at the end of tunnel excavation, causing vertical elongation of the existing tunnel.

One of reasons for the larger tunnel settlement in Test E2N3 than that in Test E2N5 (refer to Fig. 5), where the two tests had different P/Ds, was because the stress reduction at the invert of the existing tunnel was larger in the former test (see Figs 10a and 10b).

For three-tunnel interaction, incremental normal stress acting on the upper existing tunnel in case E2,3N5 (see Fig. 10c) was smaller than case E2N5. This is because the presence of the lower existing tunnel in case E2,3N5 reduced the change in normal stress at every part of the upper existing tunnel compared with that in case E2N5. In case E2,3N5, the stress reduction on the upper existing tunnel was larger in the vertical direction than that in the horizontal direction as the new tunnel advanced. This resulted in the vertical elongation of the upper existing tunnel (refer to Fig. 9a).

Figure 10d shows the incremental normal stress acting on the lower existing tunnel in case E2,3N5. Although this tunnel minimized stress redistribution in the longitudinal direction of the new tunnel, stress was still transferred in the transverse direction of the new tunnel causing stress to increase at the crown of this tunnel. At each springline, a decrease in normal stress was observed. At the invert, a sharp reduction in normal stress occurred at the completion of tunneling. As a result, the lower existing tunnel was elongated vertically (see Fig. 9a).

The allowable limits of stress change for a tunnel lining suggested by BD (2009) are shown in Figure 10. It can be seen that the change in normal stress exceeded the allowable limit of ±20 kPa in all cases. This suggests that the structural analysis considering these changes of stress acting on the tunnel linings should be taken into account.

Induced deviatoric strain of soil

Figure 11 shows the computed induced deviatoric strain of soil at the end of tunnel advancement. The positive and negative signs denote increases and decreases in deviatoric strain, respectively, compared with that prior to tunnel excavation (at 60g).

In case E2N3 (as shown in Fig. 11a), the maximum induced deviatoric strain was found at the invert of the existing tunnel directly above the new tunnel (i.e., at X/D of 0). This maximum deviatoric strain resulted in the largest reduction in soil stiffness at the centerline of the new tunnel (see Fig. 6), in addition to the largest normal stress reduction (refer to Fig. 10a).

Figure 11b shows the induced deviatoric strain in case E2N5. The magnitude of the maximum induced deviatoric strain at the invert of the existing tunnel in case E2N5 was slightly smaller than that in case E2N3 (Fig. 11a). This suggests that the smaller soil stiffness in case E2N3 than that in case E2N5 (refer to Fig. 6) was mainly due to the larger reduction in normal stress at the invert of the existing tunnel in the former case (as shown in Figs. 10a and 10b).

Induced deviatoric strain in case E2,3N5 is illustrated in Figure 11c. The induced deviatoric strain at the invert of the upper existing tunnel at the centerline of the new tunnel in case E2,3N5 was smaller than that in case E2N5. This is because the lower existing tunnel “shielded” the upper existing tunnel from the deviatoric strain induced by the new tunnel excavation. This smaller induced deviatoric strain in case E2,3N5 was another reason for the smaller reduction in soil stiffness at the invert of the existing tunnel (see Fig. 6).

Marshall et al. (2012) reported shear strain induced by a single tunnel excavation in centrifuge test. Their experimental results reveal that a zone of large shear strain occurred above the crown and shoulder of the tunnel. In case E2,3N5, the computed deviatoric strains at the crown and the shoulder of the new tunnel was smaller than that induced at the springline. This is because of the stiffening effects of the lower existing tunnel, resulting in smaller deviatoric strains at the crown and shoulder than that at the springline.

SUMMARY AND CONCLUSIONS

Three-dimensional centrifuge model tests and numerical back-analyses were conducted to investigate crossing multi-tunnel interaction. In Test E2N3, a new tunnel advanced perpendicularly beneath an existing tunnel with P/D of 0.5. Tests E2N5 and E2,3N5 were carried out to investigate the effects of the pillar depth-to-diameter ratio (P/D) and shielding on multi-tunnel interaction, respectively. Based on the interpretation of the measured and computed results, the following conclusions may be drawn:

(a) In the case of two perpendicularly crossing tunnels (one new and one existing), the measured maximum tunnel settlement at P/D of 0.5 was about 50% larger than that at P/D of 2.0. This is attributed to a smaller shear stiffness of soil in the case of P/D of 0.5 along the invert of the existing tunnel. The mobilized soil stiffness was the smallest at the location directly above the new tunnel as a result of a reduction in confining stress and an increase in deviatoric strain caused by the new tunnel excavation. The other contributing factor to the larger tunnel settlement at P/D of 0.5 is the stress acting on the tunnel lining at the location directly above the new tunnel. In the test with P/D of 0.5, stress reduction at the invert of the existing tunnel was larger than that in the test with P/D of 2.

(b) During the new tunnel excavation, induced tensile strains in the longitudinal direction of the existing tunnel and deduced shear stress on the tunnel lining were larger at P/D of 0.5 than at P/D of 2. This is due to the larger differential settlement of the existing tunnel at P/D of 0.5. These induced tensile strain and deduced shear stress at P/D of 0.5 exceeded the cracking tensile strain (ACI, 2001) and allowable shear stress (ACI, 2011), respectively.

(c) Different tunnel deformation mechanisms were observed. The existing tunnel was elongated horizontally at P/D of 0.5. This is because stress reduction on the existing tunnel in the horizontal direction was larger than that in the vertical direction. It should be pointed out that stress relief caused by the new tunnel excavation at P/D of 0.5 not only caused a reduction in vertical stress but also it resulted in substantial stress reduction at each springline of the existing tunnel. On the contrary, the existing tunnel was elongated vertically as the new tunnel advanced at P/D of 2, because stress relief was dominated in the vertical direction and it mainly affected the invert of the existing tunnel.

(d) In the case of three tunnels (two existing perpendicularly crossing tunnels above a new tunnel), the lower existing tunnel "shielded" the upper existing tunnel from the influence of the advancing new tunnel underneath, such that the measured settlement of the upper existing tunnel was 25% smaller than in the case without the shielding effects (given that P/D of 2 in both cases). This is because the lower existing tunnel reduced the effect of stress reduction and decreased deviatoric strain induced at the invert of the upper existing tunnel. These two effects resulted in a larger mobilized soil stiffness in the case of two existing tunnels than in the case of just one existing tunnel.

(e) The lower existing tunnel in the case of three tunnels was elongated vertically due to the new tunnel excavation. This is because the invert of the lower existing tunnel was closest to each section to be excavated of the new tunnel, resulting in a substantial decrease in stress in the vertical direction on the lower existing tunnel.

ACKNOWLEDGEMENTS

The authors would like to acknowledge financial support from the Research Grants Council of the HKSAR (General Research Fund project no. 617410) and would also like to thank Kelly Lim for her assistance in making the "donuts" for the centrifuge model tests.

REFERENCES

Addenbrooke, T. I. and Potts, D. M. (2001). Twin tunnel interaction: Surface and subsurface effects. *The international journal of geomechanics*, 1 (2): 249-271.

ACI (2001). Control of cracking in concrete structures (ACI 224R-01). American Concrete Institute (ACI). M.I.

ACI (2011). Building code requirements for structural concrete and commentary (ACI 318M-11). American Concrete Institute (ACI). M.I.

BD (2009). Practice note for authorized persons APP-24. Technical notes for guidance in assessing the effects of civil engineering construction / building development on railway structures and operations. Building department of the government of HKSAR (BD).

Brinkgreve, R. B. J., Engin, E. and Swolfs, W. M. (2012). PLAXIS 3D 2012 User manual. Plaxis BV, Delft.

BTS (2000). Specification for tunnelling. British Tunnelling Society (BTS). Thomas Telford, London.

Cooper, M. L., Chapman, D. N., Rogers, C. D. F. and Chan, A. H. C. (2002). Movements in the Piccadilly Line tunnels due to the Heathrow Express construction. *Géotechnique*, 52 (4): 243-257.

Garnier, J. (2001). Physical models in geotechnics: state of the art and recent advances. First Coulomb Lecture, Paris, 3 October. CFMS (eds)

Garnier, J., Gaudin, C., Springman, S. M., Culligan, P. J., Goodings, D. König, D., Kutter, B., Phillips, R., Randolph, M. F. and Thorel, L. (2007). Catalogue of scaling laws and similitude questions in geotechnical centrifuge modelling. IJPMG-*International Journal of Physical Modelling in Geotechnics* 3: 1-23.

Gudehus, G., Amorosi, A., Gens, A., Herle, I., Kolymbas, D., Mašín, D., Muir Wood, D., Nova, R., Niemunis, A., Pastor, M., Tamagnini, C. and Viggiani, G. (2008). The soilmodels.info project. *International Journal for Numerical and Analytical Methods in Geomechanics* 32 (12): 1571-1572.

Gudehus, G. and Mašín, D. (2009). Graphical representation of constitutive equations. *Géotechnique* 59 (2): 147–151.

Herle, I. and Gudehus, G. (1999). Determination of parameters of a hypoplastic constitutive model from properties of grain assemblies. *Mechanics of cohesive-frictional materials* 4: 461-486.

Hight, D. W., Gasparre, A., Nishimura, S., Minh, N. A., Jardine, R. J. and Coop, M. R. (2007). Characteristics of the London Clay from the Terminal 5 site at Heathrow Airport. *Géotechnique* 57 (1): 3–18.

Ishihara, K. (1993). Liquefaction and flow failure during earthquakes. *Géotechnique*, 43 (3): 351-415.

Jacobsz, S.W., Standing, J.R., Mair, R.J., Hagiwara, T., and Sugiyama, T. (2004). Centrifuge modelling of tunnelling near driven piles. *Soils Found.,* 44(1): 49–56.

Kim, S. H., Burd, H. J. and Milligan, G. W. E. (1998). Model testing of closely spaced tunnels in clay. *Géotechnique*, 48 (3): 375-388.

Klar, A., Vorster, T. E. B., Soga K. and Mair, R. J. (2005). Soil–pipe interaction due to tunnelling: comparison between Winkler and elastic continuum solutions. *Géotechnique*, 55(6): 461–466

LTA (2000). Code of practice for railway protection. Development and Building Control Department, Land Transport Authority (LTA), Singapore.

Mair, R. J. and Taylor, R. N. (1997). Theme lecture: Bored tunnelling in the urban environment. Proc. 14th International Conference in Soil Mechanics and Foundation Engineering, Hamburg, Balkema, pp. 2353-2385.

Marshall, A. M., Klar, A. and Mair, R. J. (2010). Tunnelling beneath buried pipes: view of soil strain and its effect on pipeline behaviour. *J. Geotech. Geoenviron. Engng*., 136 (12): 1664–1672.

Marshall, A.M., Farrell, R., Klar, A., and Mair, R. (2012). Tunnels in sands: the effect of size, depth and volume loss on greenfield displacements. *Géotechnique*, 62(5): 385–399.

Mašín, D. (2009). 3D modelling of a NATM tunnel in high K0 clay using two different constitutive models. *J. Geotech. Geoenviron. Engng*., 135(9): 1326-1335.

Mašín, D. (2012). Hypoplastic Cam-clay model. *Géotechnique*, 62 (6): 549–553.

Mohamad, H., Bennett, P. J., Soga K., Mair R. J. and Bowers, K. (2010). Behaviour of an old masonry tunnel due to tunnelling-induced ground settlement. *Géotechnique*, 60 (12): 927–938.

Ng, C. W. W. and Lee, G. K. T. (2005). Three-dimensional ground settlements and stress transfer mechanisms due to open-face tunnelling. *Can. Geotech. J.* 42: 1015–1029.

Ng, C. W. W., Van Laak, P. Tang, W. H., Li, X. S. and Zhang, L. M. (2001). The Hong Kong Geotechnical Centrifuge. Proc. 3rd Int. Conf. Soft Soil Engineering, Dec., Hong Kong. pp. 225-230.

Ng, C. W. W., Van Laak, P. A., Zhang, L. M., Tang, W. H., Zong, G. H., Wang, Z. L., Xu, G. M. and Liu, S. H. (2002). Development of a four-axis robotic manipulator for centrifuge modelling at HKUST. Proc. Int. Conf. on Physical Modelling in Geotechnics, St. John's Newfoundland, Canada, pp. 71-76.

Ng, C. W. W., Boonyarak, T. and Mašín, D. (2013). Three-dimensional centrifuge and numerical modeling of the interaction between perpendicularly crossing tunnels. *Can. Geotech. J.*, 50 (9): 935-946.

Niemunis, A. and Herle, I. (1997). Hypoplastic model for cohesionless soils with elastic strain range. *Mechanics of cohesive-frictional materials*, 2: 279-299.

Svoboda, T., Mašín, D. and Boháč, J. (2010). Class A predictions of a NATM tunnel in stiff clay. *Computers and Geotechnics*, 37(6): 817-825.

Taylor, R. N. (1995). Geotechnical Centrifuge Technology. Blackie Academic and Professional, London.

Todd, C. D. (1975). The potentiometer handbook. McGraw-Hill, New York.

von Wolffersdorff, P. A. (1996). A hypoplastic relation for granular materials with a predefined limit state surface. *Mechanics of cohesive-frictional materials*, 1: 251-271.

Yamashita, S., Jamiolkowski, M. and Lo Presti, D.C.F. (2000). Stiffness nonlinearity of three sands. *J. Geotech. Geoenviron. Engng.*, 126 (10): 929-938.

Yamashita, S., Kawaguchi, T., Nakata, Y., Mikami, T., Fujiwara, T. and Shibuya, S. (2009). Interpretation of international parallel test on the measurement of G_{max} using bender elements. *Soils Found.* 49 (4): 631–650.

Table 1 Summary of material parameters adopted in finite element analyses

Critical state friction angle[a], ϕ_c	30°
Granulates hardness[a], h_s	2.6 GPa
Exponent n[a], n	0.27
Minimum void ratio at zero pressure[a], e_{do}	0.61
Critical void ratio at zero pressure[a], e_{co}	0.98
Maximum void ratio at zero pressure[a], e_{io}	1.10
Exponent α[b], α	0.5
Exponent β[b], β	3
Parameter controlling the initial shear modulus upon a 180° strain path reversal and in the initial loading[b], m_R	8
Parameter controlling the initial shear modulus upon a 90° strain path reversal[b], m_T	4
The size of the elastic range[b], R	0.00003
Parameter controlling the rate of degradation of stiffness with strain[b], β_r	0.2
Parameter controlling the rate of degradation of stiffness with strain[b], χ	1.0
The coefficient of at-rest earth pressure, K_0	0.5

Note: (a) Adopted from Herle and Gudehus (1999)
(b) Calibrated from triaxial test results for Toyoura sand (Yamashita et al., 2000, 2009)

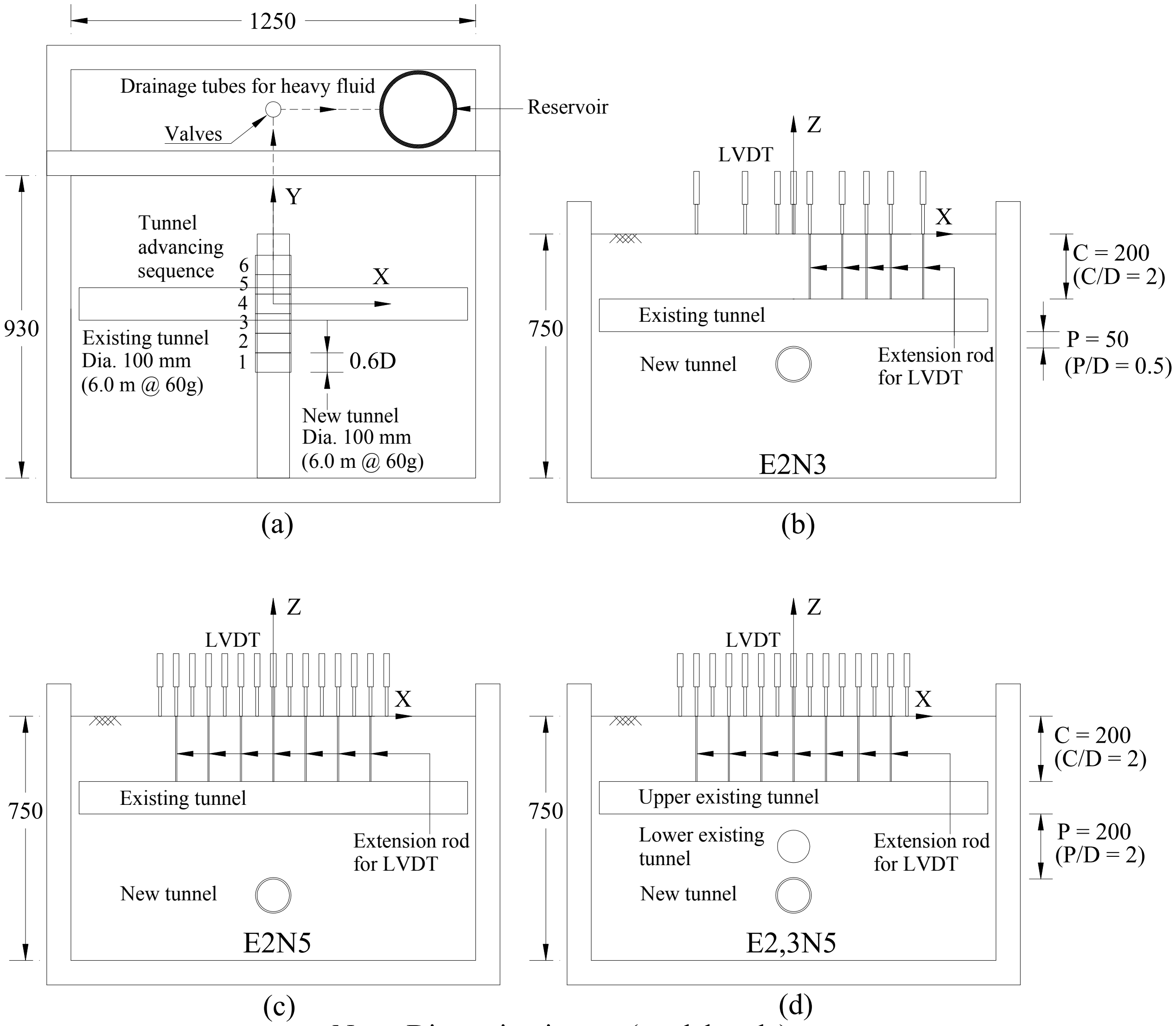

Note: Dimension in mm (model scale)

Figure 1 Schematic diagrams showing a centrifuge model package for simulating the interaction between perpendicularly crossing tunnels: (a) a typical plan view and (b) an elevation view of Test E2N3; (c) an elevation view of Test E2N5 and (d) an elevation view of Test E2,3N5

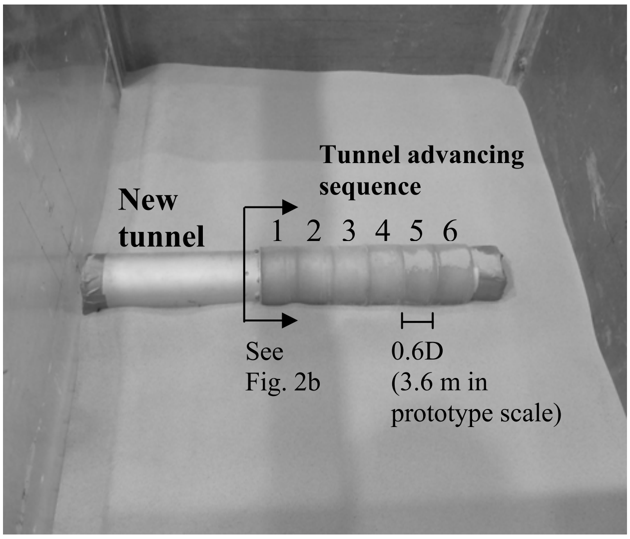

(a)

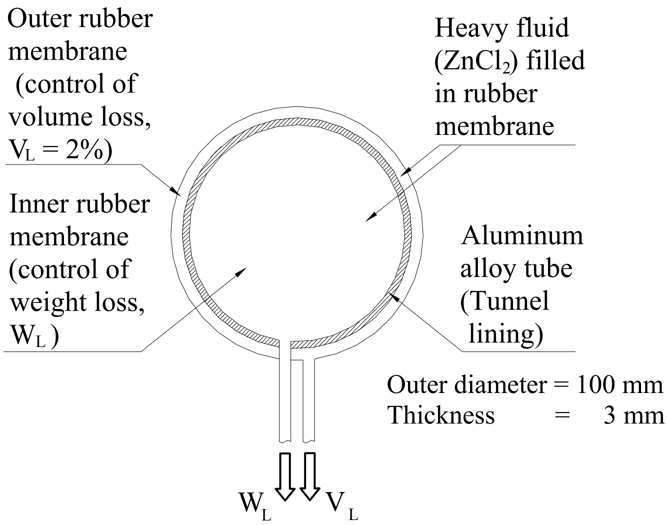

(b)

Figure 2 (a) Tunnel advancing sequence in a centrifuge test; (b) a “donut” for simulating the effects of volume loss and weight loss during tunnel excavation

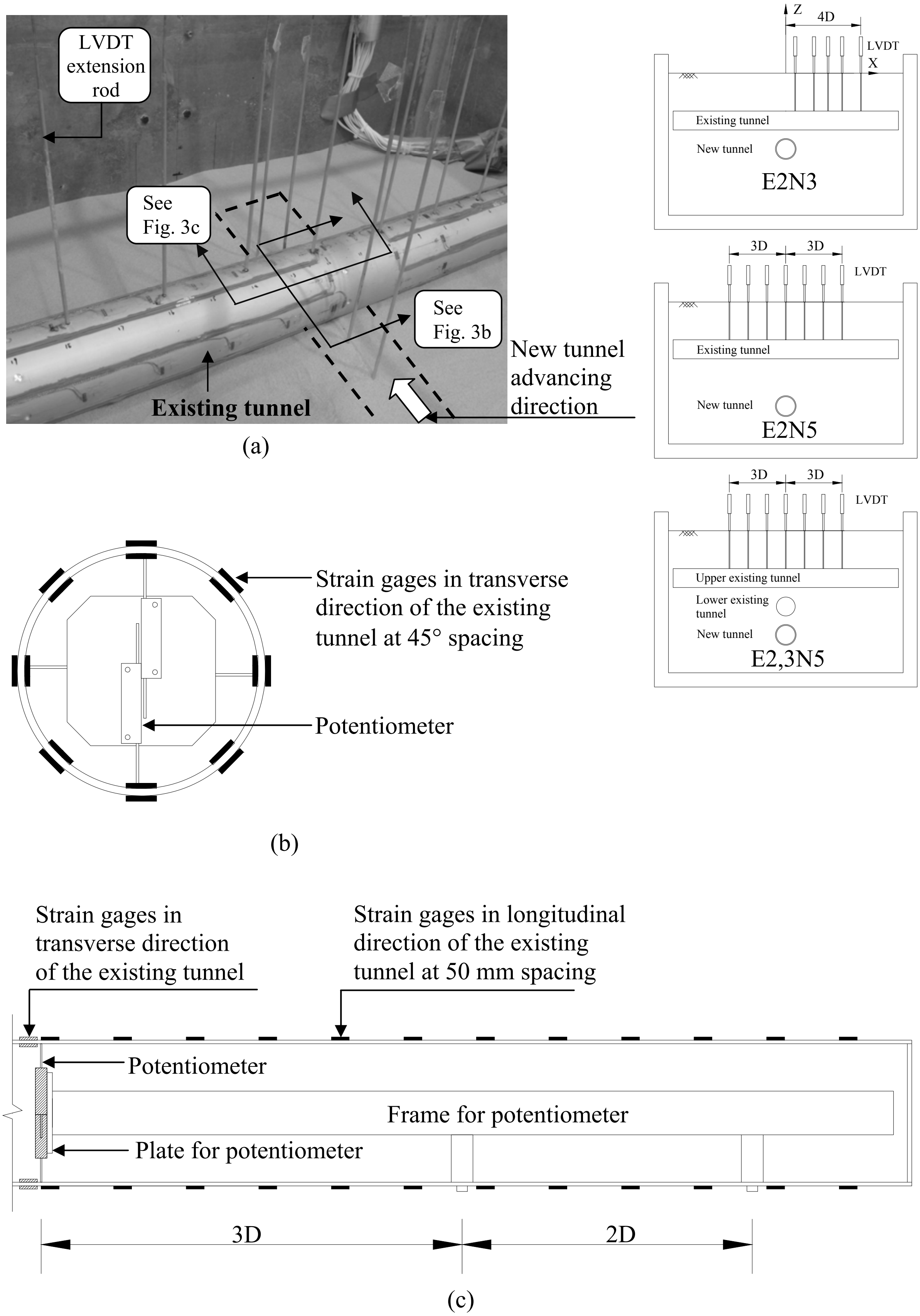

Figure 3 (a) Instruments installed at the existing tunnel; (b) transverse section view; (c) longitudinal section view

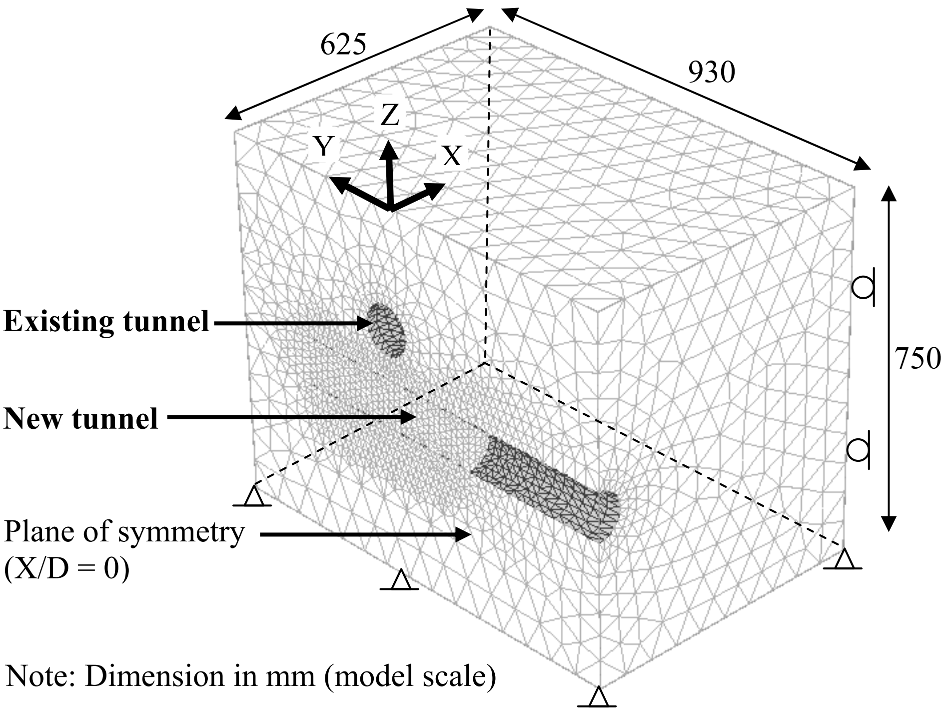

(a)

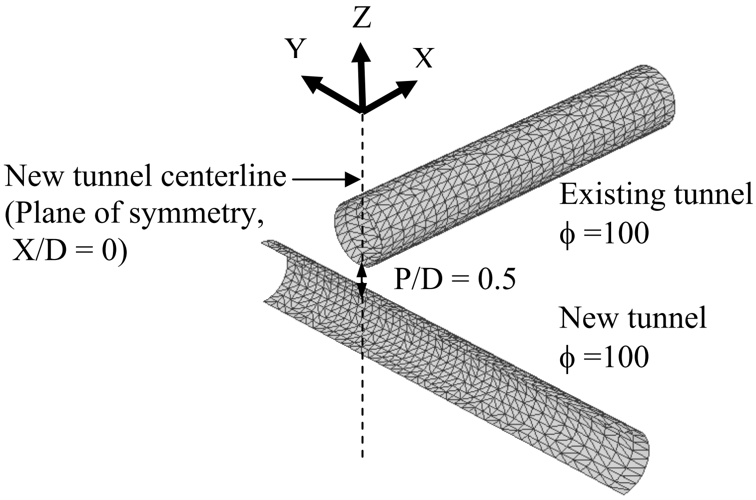

(b)

Figure 4 (a) Three-dimensional finite element mesh for case E2N3; (b) some details of the perpendicularly crossing tunnels

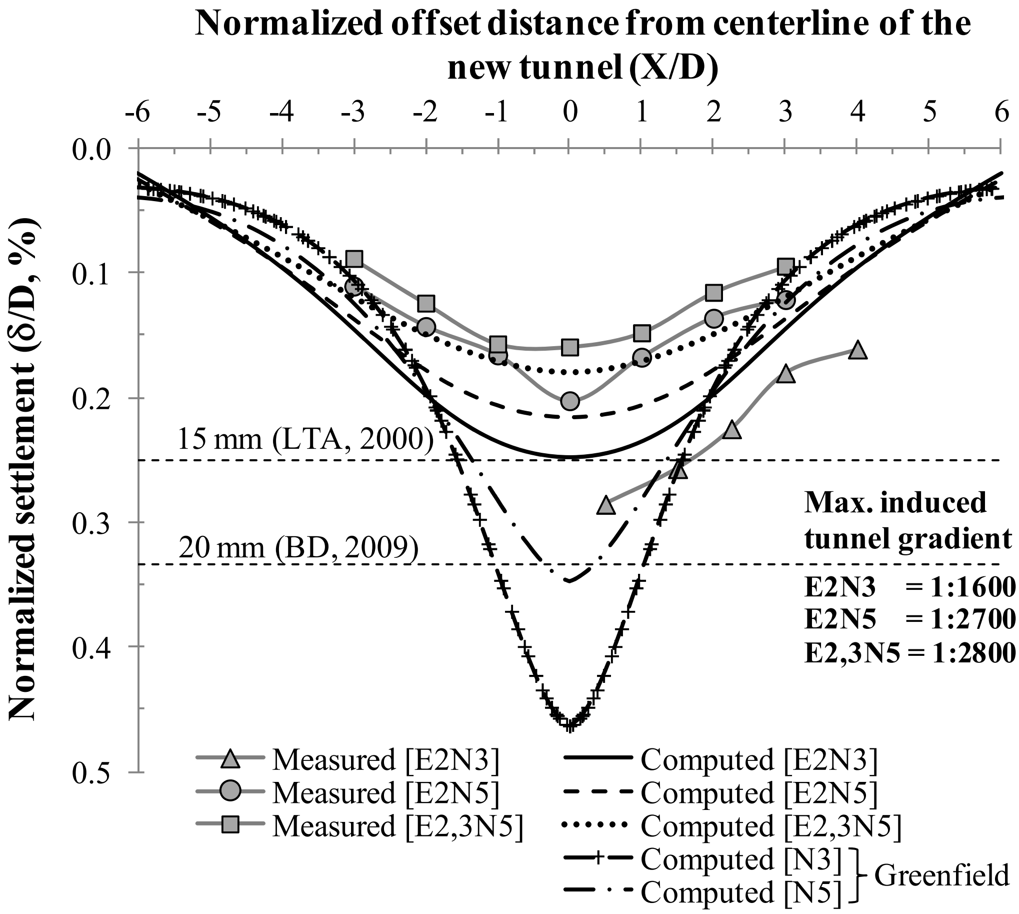

Note: In Test E2,3N5, results are shown for the upper existing tunnel only

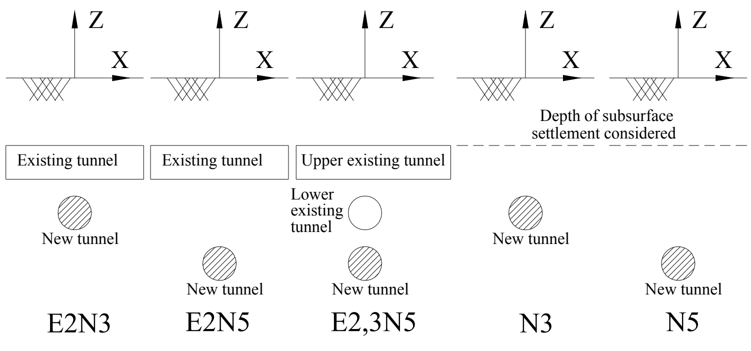

Figure 5 Comparisons of settlements of the existing tunnel and subsurface settlements in greenfield conditions

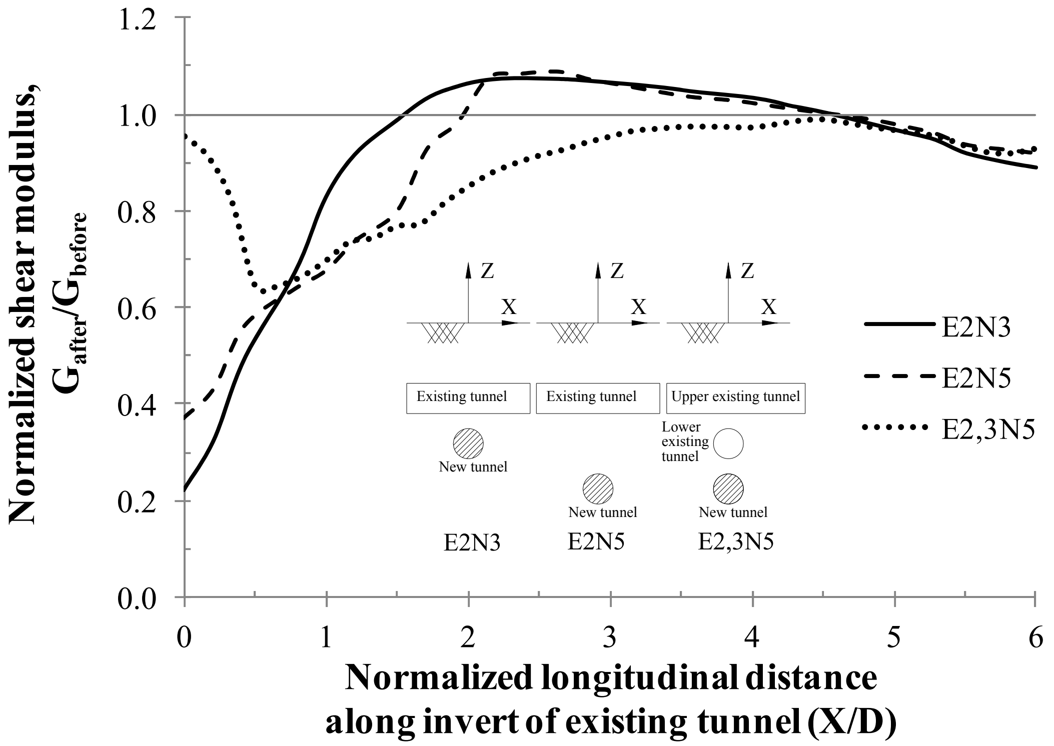

Note: In Test E2,3N5, results are shown
for the upper existing tunnel only

Figure 6 Computed normalized stiffnesses of soil (G_{after} / G_{before}) along the invert of the existing tunnel

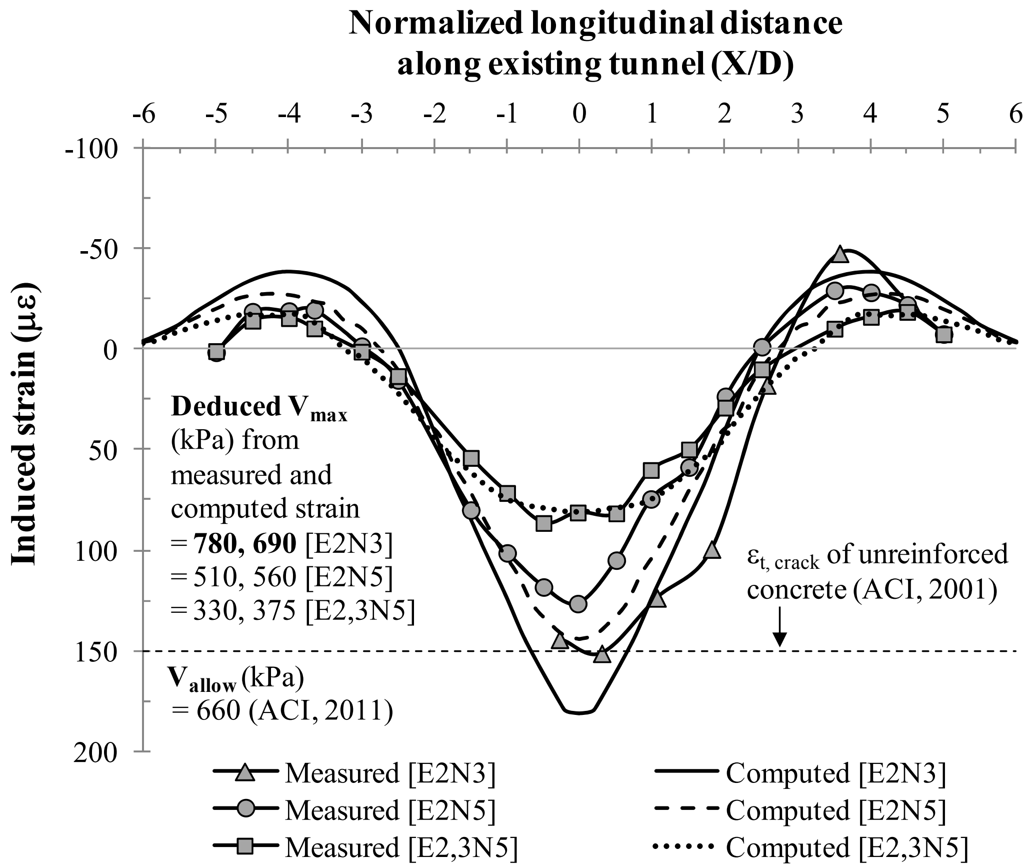

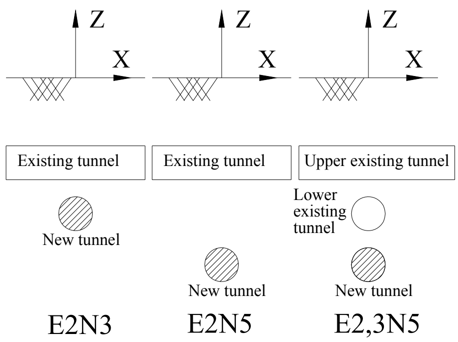

Sign convention
+ Induced tensile strain
- Induced compressive strain

Note: In Test E2,3N5, results are shown for the upper existing tunnel only

Figure 7 Induced strains in the longitudinal direction of the existing tunnel

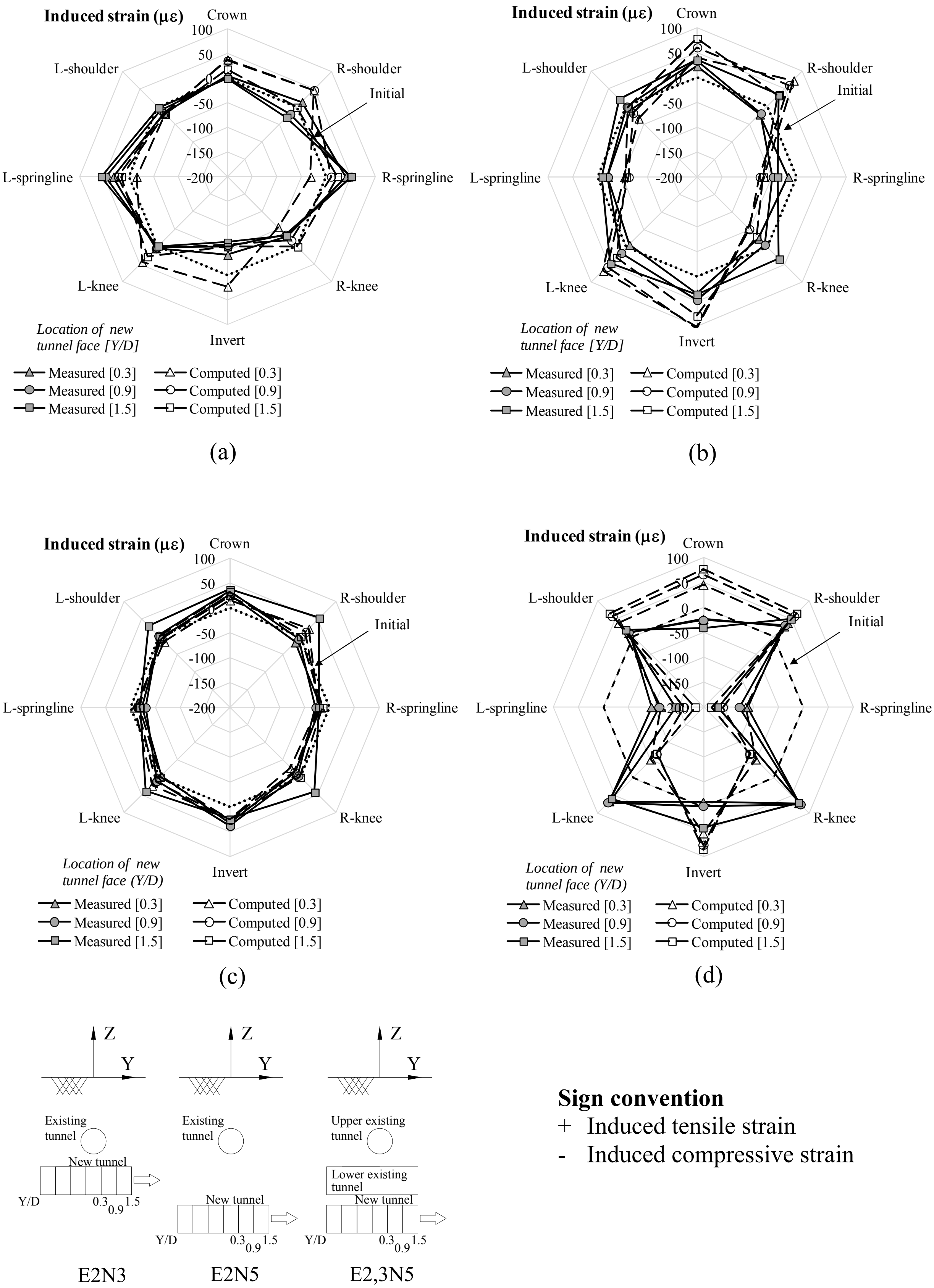

Figure 8 Comparisons of strains induced on the outer surface of the existing tunnel in the transverse direction in Tests (a) E2N3; (b) E2N5; (c) E2,3N5 upper tunnel; (d) E2,3N5 lower tunnel

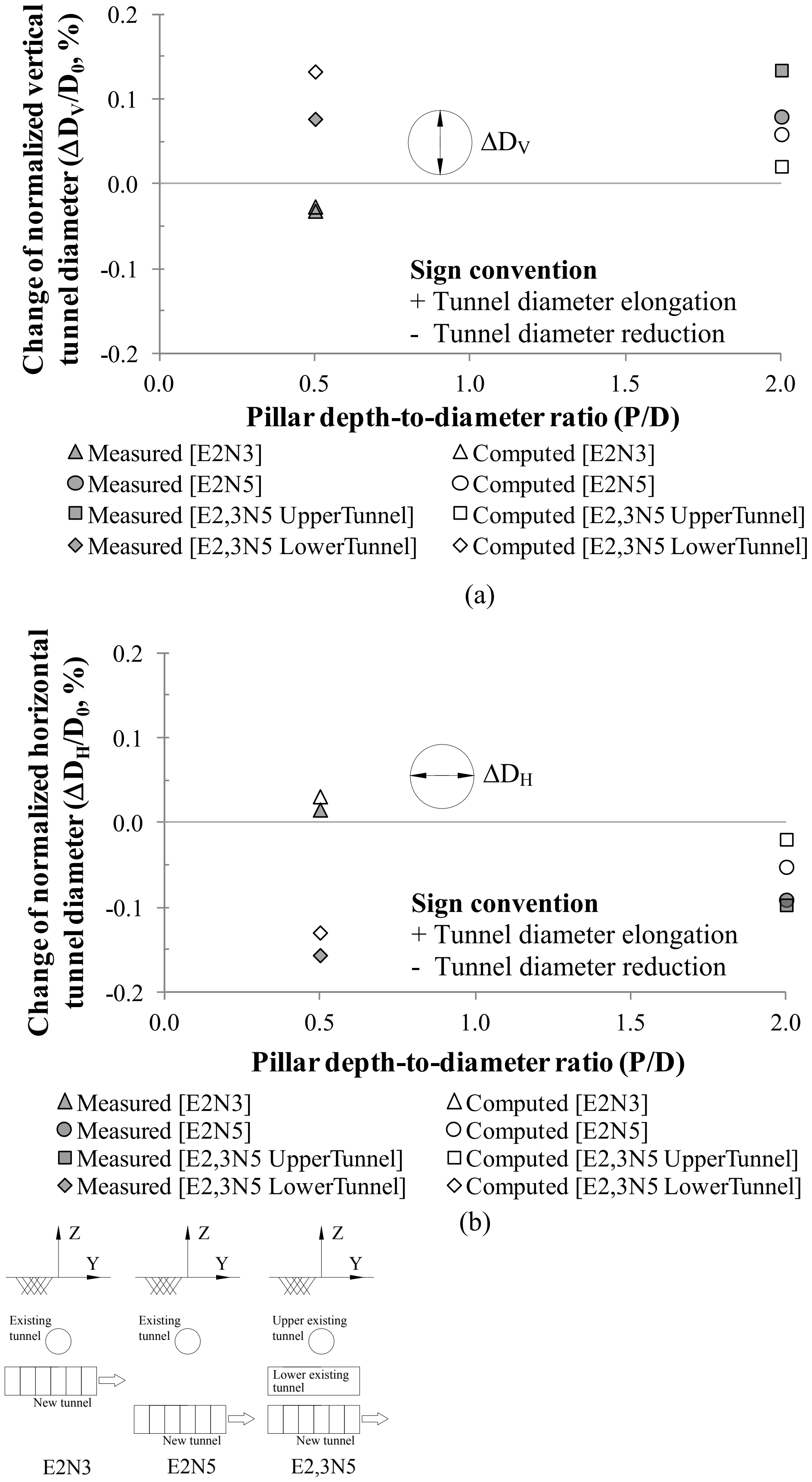

Figure 9 Deformations of the existing tunnel in (a) the vertical direction; (b) the horizontal direction

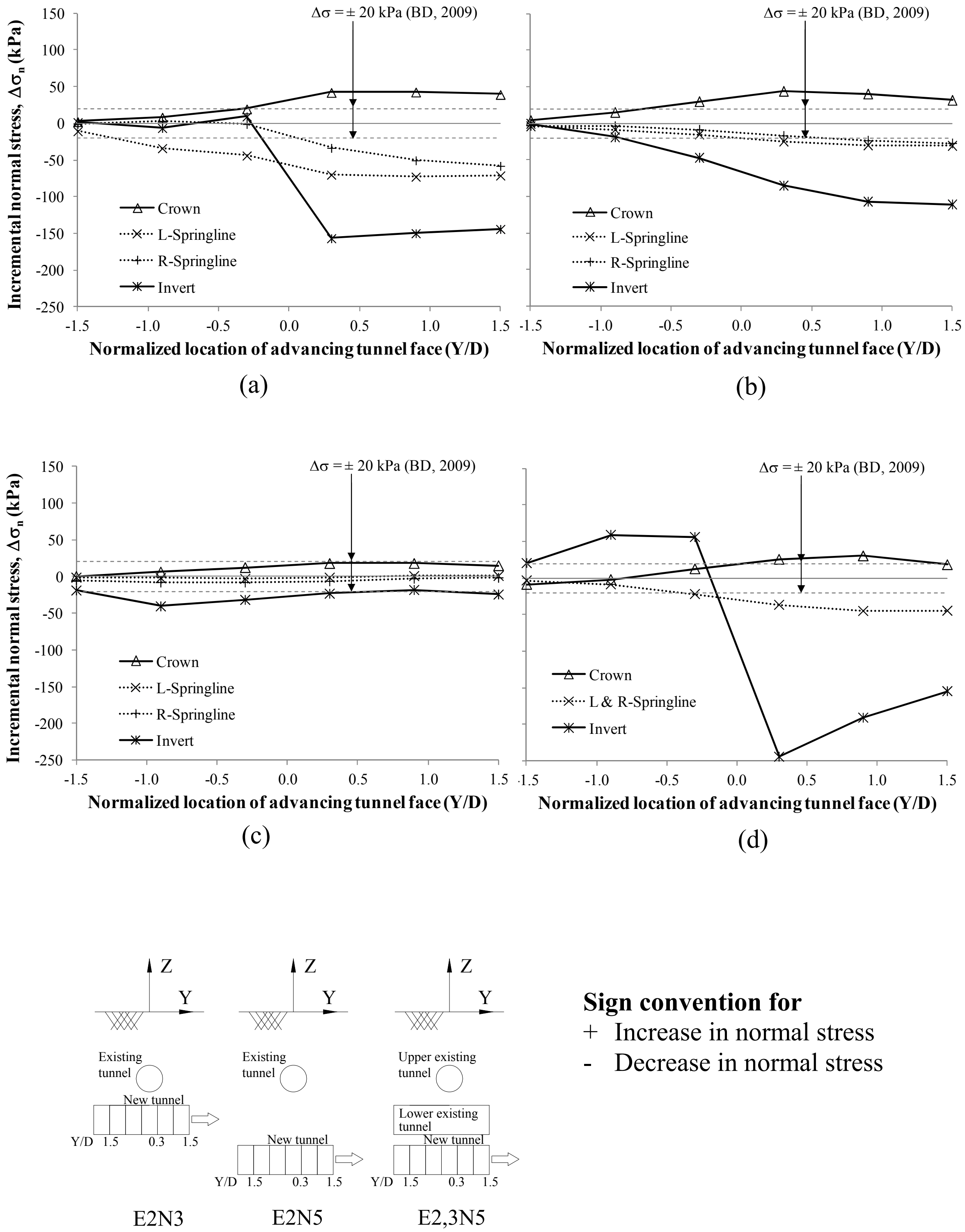

Figure 10 Computed incremental normal stresses of the existing tunnel in cases (a) E2N3; (b) E2N5; (c) E2,3N5 upper tunnel; (d) E2,3N5 lower tunnel

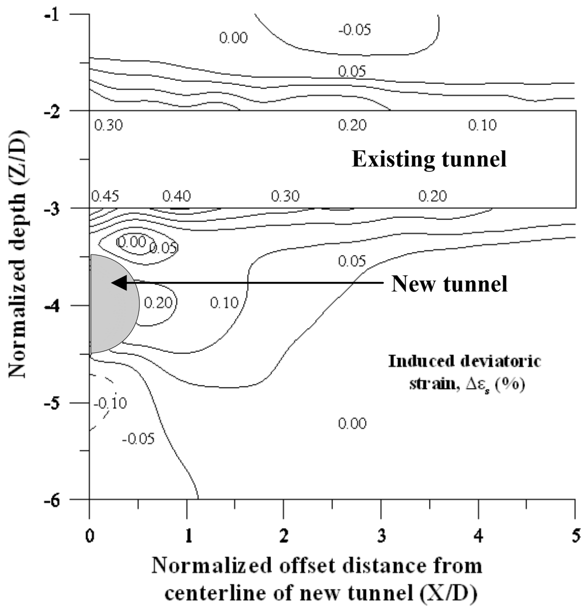

(a)

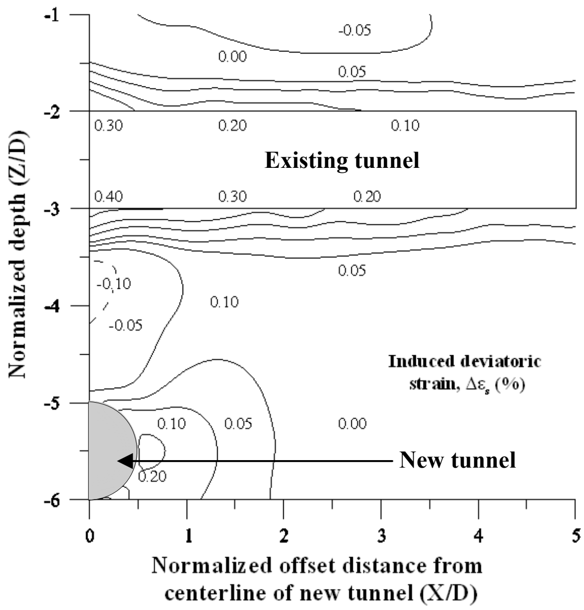

(b)

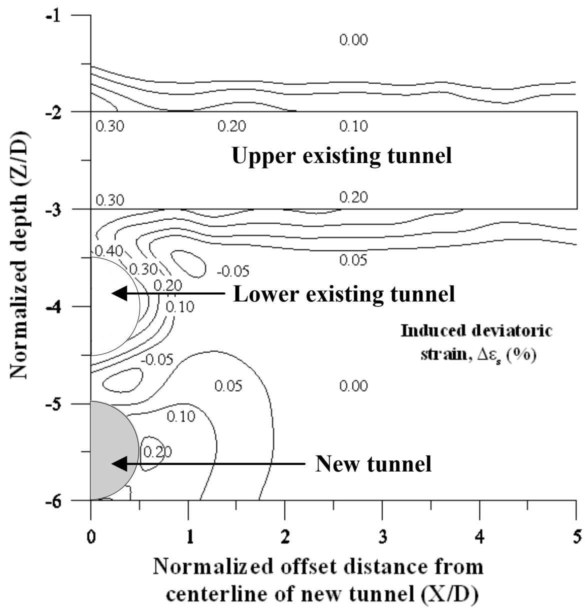

(c)

Sign convention

\+ Increase in deviatoric strain

\- Decrease in deviatoric strain

Figure 11 Contours of computed deviatoric strains induced by new tunnel excavation in cases (a) E2N3; (b) E2N5; (c) E2,3N5